

Valence electron energy-loss spectroscopy of ultrathin SrTiO₃ films grown on silicon (100) single crystal

Dong Su,^{1,a)} Bo Yang,² Nan Jiang,² M. Sawicki,³ C. Broadbridge,³ M. Couillard,⁴ J. W. Reiner,⁵ F. J. Walker,⁵ C. H. Ahn,⁵ and Yimei Zhu¹

¹Center for Functional Nanomaterials, Brookhaven National Laboratory, Upton, New York 11973, USA

²Department of Physics, Arizona State University, Tempe, Arizona 85287-1504, USA

³Department of Physics, Southern Connecticut State University, 501 Crescent Street, New Haven, Connecticut 06515, USA

⁴Department of Materials Science and Engineering and Canadian Centre for Electron Microscopy, McMaster University, Hamilton, Ontario L8S 4L7, Canada

⁵Department of Applied Physics and Center for Research on Interface Structures and Phenomena, Yale University, New Haven, Connecticut 06520-8284, USA

(Received 23 December 2009; accepted 22 February 2010; published online 25 March 2010)

Valence electron energy-loss spectroscopy is used to investigate the plasmon excitations of ultrathin SrTiO₃ sandwiched between amorphous Si and crystalline Si. Two plasmon excitations were observed, one at 15.8 eV and the other at 28.7 eV. Our calculations, based on dielectric-function theory, suggest that the former peak originates from the coupling of the Si layers and is related to the geometry of the structure, and the latter peak results from the SrTiO₃ bulk plasmon after a redshift. Our findings demonstrate the value of valence electron energy-loss spectroscopy in detecting a local change in the effective electron mass. © 2010 American Institute of Physics. [doi:10.1063/1.3364144]

Functional oxides exhibit an unparalleled variety of advantageous physical properties for electronic applications, such as high electron-mobility, high spontaneous polarization, and high superconducting-transition temperature.¹ To fully utilize these properties, it is very important to incorporate these materials into Si-based technology. SrTiO₃ (STO) thin films were grown on Si (100) single crystals without silicon oxide interfacial layers.²⁻⁴ This crystalline oxide-semiconductor system attracted much interest, especially the structural and electronic properties of the STO film close to the interface.^{5,6} However, many issues remain; for example, we do not know how the electronic structure of changes under compressive strain or with a different interfacial structure.⁷

Electron energy loss spectroscopy (EELS), together with high resolution transmission electron microscopy (TEM), offers a powerful method for exploring local electronic structure with atomic-layer precision.⁸ Recently, the valence electron energy-loss spectroscopy (VEELS) technique was applied to characterize electronic- and electromagnetic-structure at the nanoscale. For example, Nelayah *et al.*⁹ employed it to measure surface-bound optical excitations in nanoparticles; Sanchez *et al.*¹⁰ investigated the quantum dots-in-well structure using the bulk plasmon peak, and Arenal *et al.* extracted the optical gaps of single boron-nitride nanotubes using EELS. In our previous report, we proposed employing the shift of the maximum loss peak to measure the porosity of nanoporous MgO.⁹⁻¹² However, caution must be taken to link the EELS measurement with the physical properties, because of the delocalization contribution associated with plasmon excitation and because of the multiple factors that might shift the peak, such as the quantum-confinement effect, the relativistic effect, the damping effect,

and the effective response of dielectric medium.¹³⁻¹⁶

In this letter, we report our study using VEELS technique on an ultrathin STO film, sandwiched between an amorphous Si and a crystalline Si layer. We observed two predominant peaks in the low energy-loss regime within the ultrathin STO layer that do not match the corresponding peaks in the bulk STO. We undertook calculations based on dielectric theory and found that the shift of one of the main peaks in the STO layer is related to the coupling of the Si layers. We identified the other peak shift as reflecting the change in the band structure of STO.

An approximately 1 nm thin film of STO, corresponding to two and a half unit cells of STO with an (001) orientation, was grown epitaxially on a (100) Si single crystal using molecular beam epitaxy. Then, an amorphous Si layer was deposited on the STO film at room temperature. The growth sequence was optimized so that the terminal layer of STO close to the Si crystal is an Sr–O layer, [Fig. 1(a)], consistent with previous reports.^{2,17,18} We examined the specimens under a Hitachi-2700C dedicated scanning-transmission electron microscope (STEM). For these experiments, we used a

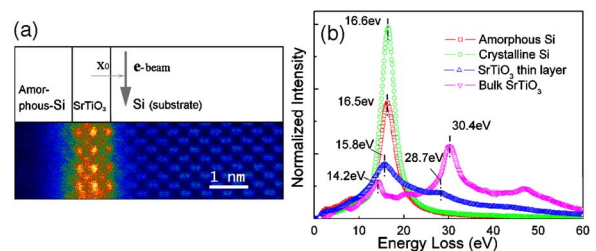


FIG. 1. (Color online) (a) Schematic view (top) and cross-sectional high angle annular dark-field image (bottom) of the sandwich structure, where x_0 indicates the position of the electron probe and $x_0=0$ sits at the center of STO thin layer. (b) Comparison of deconvoluted EELS spectra of amorphous-Si, STO thin film, crystalline Si, and bulk STO. The intensities of these spectra are calibrated with the samples' thicknesses.

^{a)}Electronic mail: dsu@bnl.gov.

1.3 Å probe with a beam current of 5 pA. EELS spectra were collected with a Gatan high-resolution spectrometer (Enfina ER), with an energy resolution of about 0.35 eV, by measuring the full width at half maximum (FWHM). All the EELS spectra were aligned to the zero-loss peak and deconvoluted using a Fourier-log method to remove the multiple-scattering effect.⁸ The relative thickness of the STO film (t/λ) was 0.55 ± 0.05 (where t is the sample's thickness and λ is total effective mean free path of the incident electrons).

Figure 1(b) plots the VEELS spectra of the amorphous Si (a-Si) layer, the STO ultrathin film, and the crystalline Si (c-Si) layer. These spectra were recorded by scanning the probe parallel to the interface. We also depict in Fig. 1(b), the reference spectrum acquired in a bulk STO sample under the same conditions. In both the amorphous and crystalline Si layers, the sharp peaks at 16.5 eV and 16.6 eV, respectively, are due to their bulk plasmon excitations. In the spectrum of the STO thin layer, we observed a small bump at ~ 8.0 eV that we attribute to coupled interface plasmon excitations.^{14,19} There are two pronounced peaks, one around 15.8 eV (peak A) and the other at 28.7 eV (peak B). Peak A is close to both the collective excitation at 14.2 eV in the bulk STO, and the plasmon peak for silicon at around 16.5 eV. We cannot derive its origin straightforwardly. On the other hand, peak B is about 1.7 eV lower than STO's bulk-plasmon peak.

In principle, the valence loss signals depend on the dielectric response. The intensity of plasmon excitations $I(\omega) \propto \text{Im}[-1/\varepsilon(\omega)] = \text{Im}[\varepsilon_2(\omega)/\varepsilon_1^2(\omega) + \varepsilon_2^2(\omega)]$, wherein $\text{Im}[-1/\varepsilon(\omega)]$ is the energy-loss function, and $\varepsilon_1(\omega)$ and $\varepsilon_2(\omega)$ are the real and imaginary dielectric constants, respectively.⁸ However, in a nanoscale structure, the geometry of the surrounding material affects the energy-loss function.^{20,21} In particular, Moreau *et al.*¹⁶ derived the relativistic expression for the excitation probability of an electron traveling parallel to a sandwiched interface. This theory was used to characterize the interface plasmon of a 2 nm thick SiO₂ layer sandwiched by silicon.¹⁹ In this study, our model assumed that 1 nm STO layer suffices to retain the dielectric property of the bulk STO, so that we can apply the dielectric response theory to our system. Accordingly, we carried out the calculations using the equations described by Moreau *et al.*, in Appendix B of Ref. 16. The real and imaginary parts of the dielectric functions were obtained from the Kramers–Kronig analyses of the spectra from bulk a-Si, bulk c-Si, and bulk STO.

We then determined the spectrum of 1 nm STO layer sandwiched within infinitely thick a-Si and c-Si layers. To evaluate t , the contribution from the sandwiched Si, we carried out the similar calculations in the same sandwiched geometry after replacing the thin STO layer with vacuum. In both models, the electron probes were set at the centers of the STO, or vacuum layer ($x_0=0$). Figure 2 shows the calculated results for these two models; for comparison, we reproduce the experimental EELS spectrum of STO layer from Fig. 1(b). In the calculated spectrum of STO layer, there are two pronounced peaks around 15 and 30 eV, approximately corresponding to peaks A and B in the experiment, respectively. However, in calculated spectrum of the vacuum layer, peak A remained but peak B disappeared. The position of peak A in the spectrum calculated for the STO layer almost matched its experimental position. Peak A in the spectrum

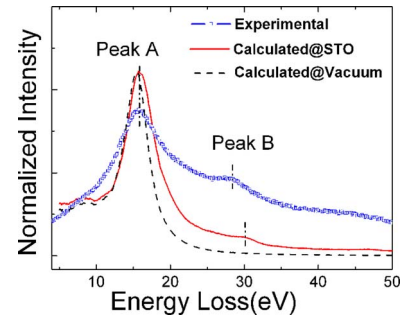


FIG. 2. (Color online) Comparison of the experimental spectrum of a-Si/STO/c-Si, the calculated spectra of a-Si/STO/c-Si and a-Si/vacuum/c-Si sandwich structures using dielectric function theory. All spectra are at the centers of the layers ($x_0=0$).

calculated for vacuum layer is about 0.4 eV lower than the peak A in the spectrum of the STO layer, implying that it originates mainly from the delocalization effect of the Si layers, but also is partially affected by the STO layer. Our detailed calculation with different widths of the vacuum layer in our a-Si/vacuum/c-Si system shows that the energy of peak A declines with an increase in the width of the vacuum layer. These findings suggested that peak A mainly is generated by the coupling of the plasmon of Si layers, and reflects the geometrical effect of the sandwiched structure.²¹ On the other hand, the fact that peak B is absent in spectrum of the vacuum layer, but appears in that of the STO layer indicates that it is associated with the STO, and can be assigned to the bulk plasmon excitation of STO. However, its position is 1.7 eV lower than that in the bulk material and in the calculated spectrum of STO layer, so we cannot interpret it as being affected by the geometric effect.

To further verify the geometric effect, we acquired spectra by moving the electron probe perpendicularly across the STO layer (from $x_0 < 0$ to $x_0 > 0$). Correspondingly, we also calculated the spectra under the same conditions with a step of 0.4 nm (from $x_0 = -3.2$ to 2.4 nm). We plot comparisons of the relative shift (to the plasmon energy of c-Si layer) of the experimental and calculated positions of peak A in Fig. 3(a), and similar comparisons of positions of peak B in Fig. 3(b). In Fig. 3(a), the calculations fit the experimental findings very well within the experimental error. Again, they confirm that peak A, observed in the STO ultrathin layer, mainly is caused by the coupling of collective excitations between c-Si and a-Si layers (the geometric effect); interestingly, both the experimental and calculated positions of peak B are little affected by the position of the electron probe within the STO thin layer [Fig. 3(d)]. This is a reasonable finding considering that the bulk dielectric data of STO are used in the calculations, and the formulae were derived based on the classical theory.

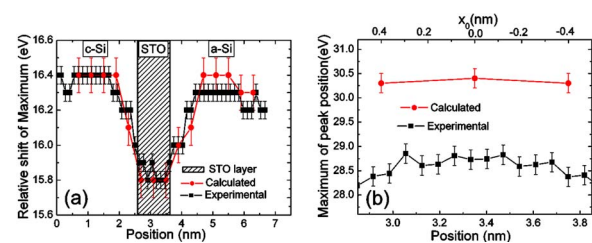


FIG. 3. (Color online) (a) Comparison of experimental and calculated values of the maximum loss position of peak A. (b) Comparison of STO plasmon peaks' positions of peak B.

Several possible mechanisms might cause a shift in the maximum-loss peak. First, we exclude the quantum confinement effect as the cause of the STO bulk plasmon shift to lower energy because this effect shifts the peak to higher energy.¹⁵ Second, as evident in Fig. 1(b), the plasmon peak of STO thin film is broader than that of the STO bulk plasmon, due to the damping effect.⁸ The strong damping effect in the ultrathin layer may shift the measured plasmon peak downwards. According to Sanchez *et al.*,¹⁰ the actual plasmon peak is at $E_p'^2 = E_{\max} \sqrt{4E_{\max}^2 + \Gamma^2} - E_{\max}^2$, where E_p' is the bulk plasmon energy, E_{\max} is the measured maximum of plasmon peak, and Γ is the damping constant that is approximately the FWHM of the plasmon peak, ΔE . Here, the contribution of band gap was considered.¹⁰ By fitting the experimental data with Gaussian function, we estimated that in the ultrathin STO layer, ΔE is ~ 9.8 eV; similarly, ΔE is estimated to be 4.6 eV for the STO bulk plasmon. Then, the corresponding energy of peak B would be ~ 0.3 eV lower than the value in STO bulk material.²² Undoubtedly, the damping effect cannot fully explain the shift of peak B in the ultrathin STO layer.

According to the Drude theory, the bulk plasmon energy is determined by the density of valence electron, n , and effective electron mass, m_{eff} , i.e., $E_p = (\hbar e / \sqrt{\epsilon_0 m_{\text{eff}}}) \cdot \sqrt{n}$.⁸ The changes of both valence electron density and effective electron mass might induce the shift in plasmon energy. As we knew, the in-plane lattice parameter of STO is 1.7% smaller than that of Si. The strain from Si compresses the in-plane lattice parameter of STO. However, the out-of-plane lattice constant of STO is elongated due to the Poisson effect. The volume change of the unit cell would be insignificant; in a similar case, the change in volume is about 0.19% for 5 ML STO layers on Si.⁵ Therefore, the energy shift due to the change in valence electron density can be negligible in our case.

The only other parameter in the equation for plasmon energy is an increase in the effective mass-tensor components in the plane crossing the electron incident beam at the electron wave vector $q \sim 0$. We calculated this enhancement as $11.5 \pm 2.0\%$, taking into account both geometrical and damping effects. To explain this enhancement, we note that the compressive strain in STO and the interfacial structure between Si and STO was shown to modify the electronic structure of STO thin films grown on silicon. For instance, density functional theory (DFT) calculations by Zhang *et al.*²³ show the valence band offset is 2.26 eV, and the offset of the conduction band is -0.13 eV. Using x-ray- and ultraviolet-photoemission spectroscopy, Amy *et al.*^{24,25} reported that the maximum position of the valence-band shifted more than 2.0 eV, depending on the surface treatment; the conduction band's minimum was below that of Si by a value from $-0.2 \sim -0.46$ eV for the STO/Si interface. The band structural change at the interface may lead to a decrease in the width of the valence state, possibly by flattening the density of states in the valence band. This mechanism is consistent with our findings on the result of the enhancement of effective electron mass in this study.

In summary, we investigated the valence electron-loss spectroscopy of a c-Si/STO/a-Si sandwiched structure. We observed two peaks at around 15.8 and 28.7 eV in the 1 nm STO ultrathin layer. Using dielectric function theory, we calculated the shifts in peaks induced by the geometry of the

sandwiched structure. The peak at 15.8 eV apparently results mainly from the coupling of Si plasmon peaks with a redshift. We can interpret the peak at 28.7 eV as an STO bulk-plasmon peak, with a 1.7 eV redshift mainly due to the enhancement of the effective electron-mass in the STO layer. Our results demonstrate that the bulk plasmon can be observed, even in a 1 nm thick film. After considering other possible effects, we consider that valence electron energy-loss spectroscopy can be a valid method to detect local changes in effective electron mass.

The work at Brookhaven was supported by U.S. Department of Energy BES under Contract No. DE-AC02-98CH10886. B.Y. and N.J. would like to acknowledge the financial support by NSF under Grant No. DMR0603993. The research of M.S., C.B., J.W.R., C.H.A., and F.J.W. was partially supported by NSF grant MRSEC under Grant No. DMR05-20495. Use of MRSEC DMR05-20495 facilities is acknowledged.

¹D. G. Schlom, L. Chen, X. Pan, A. Schmehl, and M. A. Zurbuchen, *J. Am. Ceram. Soc.* **91**, 2429 (2008).

²R. A. McKee, F. J. Walker, and M. F. Chisholm, *Phys. Rev. Lett.* **81**, 3014 (1998).

³R. A. McKee, F. J. Walker, and M. F. Chisholm, *Science* **293**, 468 (2001).

⁴H. Li, X. Hu, Y. Wei, Z. Yu, X. Zhang, R. Droopad, A. A. Demkov, J. Edwards, Jr., K. Moore, W. Ooms, J. Kulik, and P. Fejes, *J. Appl. Phys.* **93**, 4521 (2003).

⁵J. C. Woicik, H. Li, P. Zschack, E. Karapetrova, P. Ryan, C. R. Ashman, and C. S. Hellberg, *Phys. Rev. B* **73**, 024112 (2006).

⁶M. P. Warusawithana, C. Cen, C. R. Sleasman, J. C. Woicik, Y. Li, L. F. Kourkoutis, J. A. Klug, H. Li, P. Ryan, L. Wang, M. Bedzyk, D. A. Muller, L. Chen, J. Levy, and D. G. Schlom, *Science* **324**, 367 (2009).

⁷R. A. McKee, F. J. Walker, M. B. Nardelli, W. A. Shelton, and G. M. Stocks, *Science* **300**, 1726 (2003).

⁸R. F. Egerton, *Electron Energy-Loss Spectroscopy*, 2nd ed. (Plenum, New York, 1996).

⁹J. Nelayah, M. Kociak, O. Stephan, F. J. Garcia de Abajo, M. Tence, L. Henrard, D. Taverna, I. Pastoriza-Santos, L. M. Liz-Martin, and C. Colliex, *Nat. Phys.* **3**, 348 (2007).

¹⁰A. M. Sánchez, R. Beanland, M. H. Gass, A. J. Papworth, P. J. Goodhew, and M. Hopkinson, *Phys. Rev. B* **72**, 075339 (2005).

¹¹R. Arenal, O. Stéphan, M. Kociak, D. Taverna, A. Loiseau, and C. Colliex, *Phys. Rev. Lett.* **95**, 127601 (2005).

¹²N. Jiang, D. Su, J. C. H. Spence, and A. Howie, *Appl. Phys. Lett.* **94**, 253105 (2009).

¹³D. A. Muller and J. Silcox, *Ultramicroscopy* **59**, 195 (1995).

¹⁴M. Couillard, M. Kociak, O. Stéphan, G. A. Botton, and C. Colliex, *Phys. Rev. B* **76**, 165131 (2007).

¹⁵M. Mitome, H. Yamazaki, H. Takagi, and T. Nakagiri, *J. Appl. Phys.* **72**, 812 (1992).

¹⁶P. Moreau, N. Brum, C. A. Walsh, C. Colliex, and A. Howie, *Phys. Rev. B* **56**, 6774 (1997).

¹⁷S. Mi, C. Jia, V. Vaithyanathan, L. Houben, J. Schubert, D. G. Schlom, and K. Urban, *Appl. Phys. Lett.* **93**, 101913 (2008).

¹⁸L. F. Kourkoutis, C. S. Hellberg, V. Vaithyanathan, H. Li, M. K. Parker, K. E. Anderson, D. G. Schlom, and D. A. Muller, *Phys. Rev. Lett.* **100**, 036101 (2008).

¹⁹M. Couillard, A. Yurtsever, and D. A. Muller, *Phys. Rev. B* **77**, 085318 (2008).

²⁰P. Rez, X. Weng, N. J. Long, and A. K. Petford-long, *Phys. Rev. B* **42**, 9182 (1990).

²¹A. Howie, *Micron* **34**, 121 (2003).

²²The damping effect can also be calculated with equation 3.43a of Ref. 7 $E_{\max} = [(E_p)^2 - (\Delta E_p/2)^2]^{1/2}$.

²³X. Zhang, A. A. Demkov, H. Li, X. Hu, Y. Wei, and J. Kulick, *Phys. Rev. B* **68**, 125323 (2003).

²⁴F. Amy, A. Wan, A. Kahn, F. J. Walker, and R. A. McKee, *J. Appl. Phys.* **96**, 1601 (2004).

²⁵F. Amy, A. Wan, A. Kahn, F. J. Walker, and R. A. McKee, *J. Appl. Phys.* **96**, 1635 (2004).